Heterogeneous Catalysis

Deutsche Ausgabe: DOI: 10.1002/ange.201904503
Internationale Ausgabe: DOI: 10.1002/anie.201904503

Mechanism by which Tungsten Oxide Promotes the Activity of Supported V_2O_5/TiO_2 Catalysts for NO_X Abatement: Structural Effects Revealed by ^{51}V MAS NMR Spectroscopy

Nicholas R. Jaegers, Jun-Kun Lai, Yang He, Eric Walter, David A. Dixon, Monica Vasiliu, Ying Chen, Chongmin Wang, Mary Y. Hu, Karl T. Mueller, Israel E. Wachs, Yong Wang* und Jian Zhi Hu**

Abstract: *The selective catalytic reduction (SCR) of NO_x with NH_3 to N_2 with supported V_2O_5(-WO_3)/TiO_2 catalysts is an industrial technology used to mitigate toxic emissions. Long-standing uncertainties in the molecular structures of surface vanadia are clarified, whereby progressive addition of vanadia to TiO_2 forms oligomeric vanadia structures and reveals a proportional relationship of SCR reaction rate to [surface VO_x concentration]^2, implying a 2-site mechanism. Unreactive surface tungsta (WO_3) also promote the formation of oligomeric vanadia (V_2O_5) sites, showing that promoter incorporation enhances the SCR reaction by a structural effect generating adjacent surface sites and not from electronic effects as previously proposed. The findings outline a method to assess structural effects of promoter incorporation on catalysts and reveal both the dual-site requirement for the SCR reaction and the important structural promotional effect that tungsten oxide offers for the SCR reaction by V_2O_5/TiO_2 catalysts.*

Introduction

The global expansion of energy consumption has been accompanied by substantial degradation of air quality, where fossil fuel combustion is directly responsible for enhanced levels of air pollution. Among the combustion-generated air contaminants, such as sulfur oxides, carbon oxides, residual hydrocarbons, and particulate matter, nitrogen oxides (N_2O, NO, N_2O_3, NO_2, N_2O_4, and N_2O_5) are of particular concern because of their negative impact on the environment including their roles in smog, acid rain, ozone depletion, and greenhouse gases associated with climate change.[1] Growing concern for the state of the environment and human health has promoted increasingly strict regulations on the emission of NO_x, resulting in a concomitant implementation of abatement technologies.[2] The selective catalytic reduction (SCR) of nitrogen oxides by ammonia is widely practiced to mitigate NO_x emissions [see Eqs. (1) and (2)]. Although zeolite-supported Cu and Fe catalysts have recently found use in mobile applications, titania-supported vanadium oxide catalysts have been widely employed at stationary facilities and large boilers for many decades due to their relatively high activity and selectivity in the range of 300–400 °C.[3] Such stationary industrial facilities account for 40 % of the more than 107 million tonnes of NO_x released annually.[4] As SCR catalytic materials hold great importance to the preservation of the environment, a deep fundamental understanding of the mechanisms by which these reactions occur is imperative to maximizing catalyst performance by rational design of SCR catalysts. Such an endeavor requires a molecular level understanding of the catalytic system, provided by thorough characterization, for fine-tuning catalyst performance.

$$4\,NO + 4\,NH_3 + O_2 \rightarrow 4\,N_2 + 6\,H_2O \quad (1)$$

$$2\,NO_2 + 4\,NH_3 + O_2 \rightarrow 3\,N_2 + 6\,H_2O \quad (2)$$

A number of uncertainties remain regarding the SCR reaction, including the relative contributions of surface Brønsted and Lewis acid sites as the catalytic active centers[5] as well as the specific reaction mechanisms.[6] While it has been suggested that a one site Eley-Rideal (E-R)-type mechanism involving reaction between gas phase NO and adsorbed ammonia on Lewis acid sites leading to the formation of nitrosamide (NH_2NO) was consistent with the reported data[7] (see Scheme S1 in the Supporting Information), NH_3NO formation via a Langmuir-Hinshelwood (L-H)-type scheme where the adsorbed ammonia interacts with weakly or briefly adsorbed NO has also been proposed over

[*] N. R. Jaegers, Y. He, E. Walter, Y. Chen, C. Wang, M. Y. Hu, K. T. Mueller, Y. Wang, J. Z. Hu
Institute for Integrated Catalysis and Earth and Biological Science Directorate
Pacific Northwest National Laboratory
Richland, WA 99354 (USA)
E-Mail: yong.wang@pnnl.gov
Jianzhi.hu@pnnl.gov
N. R. Jaegers, Y. Wang
Voiland School of Chemical Engineering and Bioengineering
Washington State University
Pullman, WA 99163 (USA)
J.-K. Lai, I. E. Wachs
*Operando*Molecular Spectroscopy & Catalysis Laboratory
Lehigh University
Bethlehem, PA 18015 (USA)
E-Mail: iew0@lehigh.edu
D. A. Dixon, M. Vasiliu
Department of Chemistry, The University of Alabama
Tuscaloosa, AL 35487 (USA)
Supporting information and the ORCID identification number(s) for the author(s) of this article can be found under: https://doi.org/10.1002/anie.201904503.

two sites (either for adsorption of both NH_3 and NO or to facilitate N–H bond activation, Scheme S2).[6–8] Isotopic $^{18}O_2$ labeling experiments with molecular O_2 have further confirmed that a Mars-van Krevelen (MvK) mechanism also operates, where the oxygen participating in the SCR reaction is supplied by the surface vanadia (V_2O_5) sites and the catalytic cycle is completed by reoxidation of the reduced surface vanadia species from gas phase molecular O_2.[8d,9] The MvK mechanism, however, does not distinguish between the participation of one or two catalytic active sites in the SCR reaction.

Complementary to exploring the reaction pathways for chemical transformations, investigations into the catalytic active sites hold great importance for rationally guiding the design of catalysts with improved performance. Selection of promoters, surface vanadium oxide and promoter loading, method of preparation, and even the chemical environment have been shown to impact SCR performance.[3,10] Tungsten oxide is a widely used promoter for supported V_2O_5/TiO_2 catalysts because its addition, enhances measured Bronsted acidity, increases SCR activity, broadens the operational temperature range, improves the product selectivity, reduces active site poisoning propensity, and stabilizes the catalyst against thermal sintering, especially in the presence of surface vanadia that has a propensity for sintering of the TiO_2 support.[6,11] These effects demonstrate the importance of catalyst formulation on the interactions between the surface metal oxide sites and reacting substrates, and have given rise to multiple explanations for the improvements in performance by addition of tungsten oxide. However, it has been debated over the years whether the promotion of SCR reactivity takes place via a structural effect or an electronic effect which modifies the redox properties of vanadia through effects such as induction, conjugation, or electronic spin state.[6]

The nature of the surface vanadia active sites on TiO_2 supports has received much attention to facilitate an improved understanding of the relationship between the molecular structures of the catalytic active sites and SCR activity and selectivity. Among spectroscopic techniques (including IR,[7] Raman,[12] and UV/Vis[13]) difficulties exist in providing a quantitative illustration of the distribution of the surface vanadia sites. Molecular structural assignments of the surface vanadia sites on promoted oxide supports are even more challenging due to signal overlap. As such, molecular level understanding is still critically needed for further development of fundamental structure–function relationships for the SCR reaction by promoted, supported V_2O_5/TiO_2 in order to clarify the role of promoters and provide guidance for rationally improving SCR catalysts. To overcome the shortfalls of other spectroscopic techniques (e.g., IR, Raman, UV/Vis and XAS), high-field ^{51}V solid-state magic angle spinning (MAS) nuclear magnetic resonance (NMR) can be used to probe catalytic materials to elucidate the structural environment around the surface vanadia catalytic active sites.[14] Previous technological limitations in the magnetic field, sample spinning rate, and spectral interpretation have impaired a detailed analysis of the surface vanadia sites present on oxide supports.[15] When sufficiently high fields and fast spinning rates are applied, it has now become possible to distinguish between unique surface vanadia sites on titania for enhanced species identification and quantification.[14a]

Herein, we combine detailed in situ spectroscopic measurements (MAS NMR, Raman, electron paramagnetic resonance (EPR)), quantum chemistry electronic structure calculations, and catalytic kinetic studies, to clearly demonstrate that incorporation of the tungsten oxide promoter improves the SCR catalytic activity by altering the molecular structure of the surface vanadia sites to configurations favorable to SCR of NO_x by NH_3. This research strategy has provided direct evidence, for the first time, of the molecular structural changes that occur on the surface vanadium oxide active centers in the presence of the surface tungsten oxide promoter, demonstrating that the promotion mechanism of tungsten oxide proceeds via a structural effect and not as an electronic effect as widely proposed in the literature. Such a strategy offers a template for evaluating potential structural impacts of catalyst promoters for an array of applications.

Results and Discussion

Unpromoted V_2O_5/TiO_2

Although the TiO_2 support has been shown to have negligible activity for the SCR reaction at relevant reaction conditions, it is important for activation of the surface vanadia sites (support effect).[7,16] Only upon vanadia deposition do the supported V_2O_5/TiO_2 materials demonstrate catalytic function towards the abatement of nitrogen oxides via the SCR reaction with ammonia. The changes in SCR reactivity upon progressive addition of vanadia onto a TiO_2 support are illustrated in Figure 1. The reaction rate ($mol\,g^{-1}$ cat-s) is shown to steadily increase with the addition of vanadia onto the TiO_2 support up to 5% V_2O_5/TiO_2 (monolayer coverage). More than a 30-fold increase in the reaction rate is observed by increasing the vanadium oxide loading from 1% to 5% V_2O_5 on the TiO_2 support, which indicates a strong relation

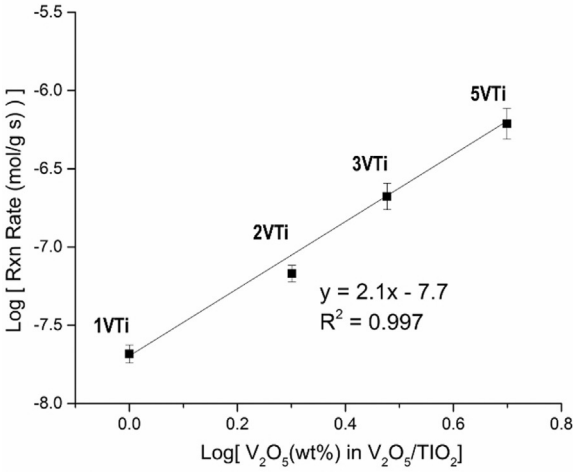

Figure 1. A plot of the log [reaction rate] versus log [vanadium oxide loading] (*x* axis) reveals a slope of 2, suggesting the preference for two surface vanadia sites in close proximity for the SCR reaction. Reactions were conducted at 200 °C.

between the quantity of surface vanadia sites and the SCR reaction rate. This observation is preserved when considering the specific SCR turnover frequency (TOF, molecules of NO converted per vanadia site per second), since a 6-fold increase in TOF is observed over a 5-fold enhancement of surface vanadia loading below monolayer coverage, which indicates that the surface vanadia sites are more effective at the SCR reaction at higher loadings (see Figure S1). It should be noted that at higher vanadia loadings, side reactions, such as ammonia oxidation, become relevant, which negatively affect the observed reaction rate as observed previously (>3% V_2O_5, selectivity N_2 ca. 85%; >7% WO_3, selectivity N_2 ca. 91%).[7,12c] Considering this reactivity in the context of a plot of log [reaction rate] vs. log [VO_x loading], where all the vanadia sites are exposed as surface sites, a slope of approximately 2 is found, indicating that the SCR reaction rate varies as the square of the concentration of surface vanadia sites ($[VO_x]^2$), which suggests that the reaction involves two surface vanadia sites.

To better understand the observed SCR activity trend with surface vanadia site coverage, detailed characterization studies were undertaken to examine the dehydrated molecular structure of the catalytic surface vanadia active sites on the TiO_2 support. The X-ray diffraction pattern (Figure S3) demonstrates the absence of large (>3 nm) V_2O_5 crystallites and only contains the diffraction patterns for the anatase (84%) and rutile (16%) phases of TiO_2 initially present in the parent TiO_2 support, which is confirmed by high-resolution transmission electron microscopy revealing the abundance of anatase TiO_2. The electron diffraction pattern also confirms a dominating anatase phase Figure S6b, with a minor rutile component that largely overlaps with anatase, except at 3.26 A where the rutile 110 ring is lightly visible. Analysis of the supported 5% V_2O_5/TiO_2 catalyst by high-resolution scanning transmission electron microscopy (STEM) coupled with electron energy loss spectroscopy (EELS) (Figure S5–S7) confirms the high dispersion of vanadia due to its presence along all probed edge positions. Non-edge vanadium detection is hindered by titania thickness whereas exterior edge detection is enhanced by both a thinner support and a higher abundance of vanadia aligned parallel to the electron beam, enhancing the EELS signal.[17] It should be noted that TiO_2 edges, where the support is thinner, allows detection of vanadia by EELS (Figure S5d–f and Figure S7), and demonstrates an expansion of the lattice spacing when surface vanadia is anchored on the TiO_2 support (from 3.35 to 3.91 Å on [0$\bar{1}$1]). This demonstrates the strongVO_X-TiO_2 anchoring interaction resulting in reconstruction the TiO_2 support surface.

For promoter-free supported V_2O_5/TiO_2 catalysts, Raman spectroscopy has been extensively used to elucidate the nature of the surface vanadia sites and their transformation during dehydration from ambient to dry conditions, with the latter state dominating during the SCR reaction at elevated temperatures because of the rapid desorption of moisture from the catalyst surface.[12b,c,18] The corresponding in situ Raman spectra (Figure S4 and associated discussion) of the bare TiO_2, supported 1% V_2O_5/TiO_2, and supported 5% V_2O_5/TiO_2 exhibit the formation of the vanadyl (V=O) bond of surface VO_4 sites (1032 cm^{-1}).[6] This terminal V=O band slightly blue shifts with increasing surface vanadia coverage owing to vibrational coupling of adjacent V=O bonds, which provides evidence for oligomerization of the surface vanadia sites with increasing surface vanadia coverage[10h,12b,19] and is associated with the concomitant lowering of the apparent activation energy of the SCR reaction.[8a,13,20] The maximum dispersion of the two-dimensional surface vanadia sites on titania is reached at a monolayer coverage (ca. 8 V nm^{-2}), with additional vanadia loading forming crystalline V_2O_5 nanoparticles that are less active than the surface vanadia sites.[12a] The absence of a Raman band from crystalline V_2O_5 nanoparticles (995 cm^{-1}) reveals that the vanadia in these catalyst samples are 100% dispersed on the titania support.

Solid-state ^{51}V MAS NMR spectroscopy was employed to provide direct information about the molecular structures of the dehydrated surface vanadia sites as a function of vanadia coverage. The in situ ^{51}V MAS NMR spectra for the dehydrated supported V_2O_5/TiO_2 catalysts in the center-band region are displayed in Figure 2, demonstrating that the vanadia structure is more complex than on silica (Figure S10).[14] Full sideband patterns at 14 and 20T are visible in the Supporting Information, where differences in spectral signals are related to spinning rate-induced separation of side bands and slight quadrupolar broadening effects. Although NMR spectroscopy can only detect V^{5+} species, the contributions from V^{+4} paramagnetic species can be detected with Electron Paramagnetic Resonance (EPR) spectroscopy (Figure S13). The EPR measurements found that V^{+4} species are minimal and account for no more than 1% of the total vanadium in the catalysts of this study (Table S1). As such, the NMR observations provide a description of nearly all vanadium oxide sites on the titania support.

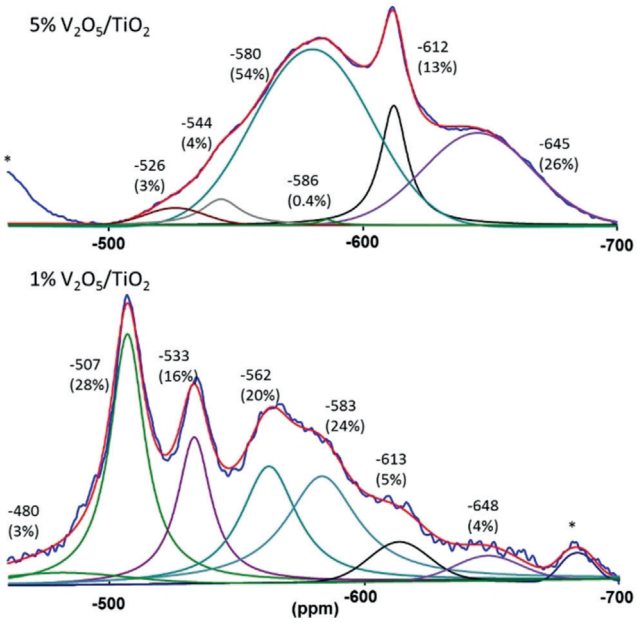

Figure 2. ^{51}V MAS NMR spectroscopy results of dehydrated, supported V_2O_5/TiO_2 catalysts prepared by impregnation. Spectral deconvolution summation is presented by the red line and the collected data in blue. Sidebands displayed are indicated by (*).

Comparison of the 1% V_2O_5/TiO_2 (ca. 0.2 monolayer coverage) and the 5% V_2O_5/TiO_2 coverage (ca. 1 monolayer coverage) catalysts reveals apparent, distinct structural differences. The supported 5% V_2O_5/TiO_2 catalyst primarily contains features below the ^{51}V NMR −544 ppm peak (96%), similar to those we previously reported.[14a] A relatively narrow feature at −612 ppm accounts for 13% of the total vanadia species in the supported 5% V_2O_5/TiO_2 catalyst that is the approximate position of V_2O_5-like nanoparticles, but may also be related to large, 2D oligomeric surface vanadia structures at these higher loadings. Small quantities of this signal also appear to be present (ca. 6%) even for the supported 1% V_2O_5/TiO_2 catalyst, as previously reported,[14a] further suggesting that these signals may belong to large oligomers. Raman spectroscopy is highly sensitive to V_2O_5 crystallites that are not observed even in the supported 5% V_2O_5/TiO_2 catalyst, highlighting the complementary nature of the two spectroscopic techniques.

For the dehydrated supported 5% V_2O_5/TiO_2 catalyst (about monolayer coverage), the solid state ^{51}V MAS NMR spectrum exhibits a broad peak at −645 ppm accounting for nearly 26% of the vanadium oxide and was previously assigned to dimeric and linear oligomeric surface vanadia sites.[14a] Peaks in this region also display a strong side band pattern. Downfield of −612 ppm, the features between −550 and −590 ppm account for about 54% of the total vanadia and two smaller peaks at −526 and −544 ppm account for the remaining 7%. The solid state ^{51}V MAS NMR spectrum of the dehydrated supported 1% V_2O_5/TiO_2 catalyst (ca. 0.2 monolayer coverage), however, only possesses 4% of the vanadia at −645 ppm corresponding to oligomeric species. This catalyst with lower surface coverage possesses a wider array of low field signals, with a broad line at −480 ppm and two distinct lines at −507 and −533 ppm that account for nearly half of the surface vanadia sites. Interpretation of these ^{51}V MAS NMR signals is based on prior assignments and our new electronic structure calculations.

Much of the prior literature was limited by low magnetic field strength, slow spinning rates, or wide-line spectra where only a couple of signals were detected. For instance, a line at −555 ppm was originally assigned to a distorted VO_4 structures and a line at −510 ppm was assigned to a distorted VO_6 structure; with the VO_4 coordination also reported at −530 ppm.[21] The most extensive investigation of the ^{51}V MAS NMR signals for titania-supported vanadia catalysts was recently conducted under high-field and fast spinning rates, and supported by electronic structure calculations of the chemical shifts on small cluster models of various vanadium oxide species.[14a] The results suggested the presence of monomeric surface vanadia sites with lines at −502 and −529 ppm, dimeric surface vanadia sites with lines at −555 ppm and −630 ppm, with the latter arising from dimeric structures with one V−O−V bond as well as linear oligomeric surface vanadium oxide chains, and signals near −610 ppm ascribed to highly oligomerized vanadia species such as crystalline V_2O_5-like nanoparticles.

The previously utilized cluster models to evaluate nuclear shielding showed good agreement with the experimental data provided, but not all peaks could be assigned based on these models.[14a] Additionally, the role of facet-dependent structures is currently being debated.[22] Since the titania surface in the previous calculations was not constrained to any specific crystallographic structure, but was fully relaxed in the cluster models, such cluster models may not account for subtle structural differences present when surface vanadia species are anchored on the low index facets often exposed and observed to dominate on these TiO_2 particles. High index anatase facets are present and 14% of the sample is rutile TiO_2, but anatase (101) and (001) were the most abundantly observed, promoting their use in DFT modeling. To consider the impact of the anchoring facet, additional models of surface vanadia anchored to anatase (101) and (001) surfaces were constructed (see Figure 3) for use in the electronic structure calculations.

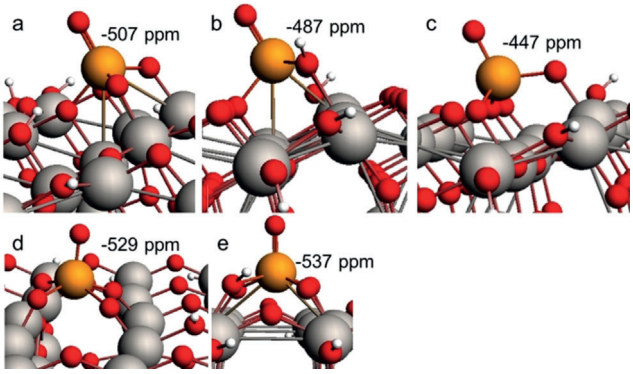

Figure 3. DFT clusters used to model monomeric structures on TiO_2, including distorted VO_4 (a), distorted VO_4 with bridge bond protonation (b), distorted VO_4 using two oxygen from TiO_2 (c), distorted square pyramidal (d), and distorted square pyramidal with bridge bond protonation (e). V orange, Ti gray, O red, and H white.

Periodic density functional theory (DFT) calculations have suggested that distorted VO_5 environments are relatively more stable on the (001) facet where anchoring is preferred, but distorted VO_4 structures dominate on (101).[23] Our monomeric models for the (101) surface reflect distorted VO_4 structures (Figure 3 a–c) that provide a calculated shift of −506 ppm and −487 ppm for structures with protons placed on nearby titania and on the bridging V−OH−Ti bond, respectively. These protons charge-balance the DFT cluster and are justified by the generation of Brønsted acidity as vanadium oxide atoms titrate surface titanol sites.[5b] Indeed, signals at the first two values are observed for the vanadia-only catalyst impregnated on TiO_2 (−507 and −480 ppm). Structures on the (001) surface optimized to yield five-coordinate vanadium atoms are depicted in (Figure 3 d,e). Again, two structures which differ only by the placement of the proton show promise on the basis of chemical shift and the reported formation energies reported by Du et al.[23a] These peaks are at −529 ppm (Figure 3 d) and −537 ppm (Figure 3 e, which is the preferred configuration at high surface vanadia coverage[23b]) and are likely candidates for the −533 ppm peak observed in the NMR spectra. This peak has been previously ascribed to various surface vanadia structures, but these new DFT calculations show strong support for a monomeric-type

surface vanadia assignment.[14a,21a,b] The low-field broad signal at −480 ppm may be related to surface vanadia sites anchored near oxygen-vacant titania, where modeling predicts nuclear deshielding by about 25 ppm (see Figure S14), but the slightly altered configuration from Figure 3c may be related. On the basis of the computational and ^{51}V MAS NMR experimental results, we can assign the low-field ^{51}V MAS NMR peaks as an array of monomeric species present on the titania surface: distorted VO_4 with a nearby OH or oxygen vacant VO_4 (−480 ppm), disordered VO_4 (−507 ppm), and distorted VO_5 (−533 ppm). Dimeric surface vanadia structures are predicted to resonate at −639 and −553 ppm for mono- and di-linked structures, respectively.[14a] Differences were also noted for oligomeric chains of surface vanadia species where the small cluster models predicted shifts near −630 ppm. The present study predicts somewhat different chemical shifts for internal and terminating vanadium atoms in polyvanadate chains, with the outer vanadium atoms predicted at −663 ppm and the inner vanadium atoms at −633 ppm. The observed expansion of the lattice spacing of TiO_2 edges when vanadia is anchored (Figure S5 d–f and Figure S7 from 3.35 to 3.91 Å on [0$\bar{1}$1]) is consistent with our DFT predictions of expansion for the four local Ti atoms around monomeric surface vanadia (3.45 to 4.33 Å on [001]). The Raman spectral results, coupled with the minimal abundance of low-field ^{51}V MAS NMR signals at higher loading where larger domains are preferred, allow us to conclude that the broad signals in the −640 ppm region retain their assignment to dimeric and oligomeric surface vanadia structures. As such, surface VO_x monomers account for approximately 47% (shifts downfield of −540 ppm) of the surface vanadia sites at low coverage (ca. 0.2 monolayer) and only about 3% of the surface vanadia sites at high coverage (monolayer) on the TiO_2 support. In contrast, dimeric and oligomeric surface VO_x sites on TiO_2 support (shifts of −560 to −580 and peaks below bulk V_2O_5) represent 48% of the surface vanadia sites at low coverage and 80% of the surface vanadia sites at monolayer coverage. These trends reflect the oligomerization of surface vanadia sites on the TiO_2 support with increasing surface vanadia coverage, supporting the established notion of increasing oligomerization of surface vanadia sites at higher surface coverage since these upfield signals are present in the supported 5% V_2O_5/TiO_2 catalyst. Based upon the prior work[14a] and the current interpretation based on the electronic structure calculations, we have confirmed that surface vanadia sites become increasingly oligomeric as the surface vanadium oxide loading increases; the increase in surface loading also results in a higher specific catalytic activity (TOF). These spectroscopic observations support the observation that the SCR of NO_x with NH_3 involves two adjacent surface vanadia sites in close proximity (see Figure 1 and associated discussion).

Promoted V_2O_5-WO_3/TiO_2

Although supported V_2O_5/TiO_2 catalysts effectively catalyze the SCR of NO with NH_3 reaction, incorporation of tungsten oxide as a promoter provides a number of benefits such as the excellent thermal stability, lower activity for sulfur oxidation, and improved SCR activity.[7,24] These improvements also include an increase in the number of Brønsted and Lewis acid sites and their corresponding acid strengths, ammonia adsorption capacity, and enhanced reducibility of surface vanadia sites.[11a,25] Supported $V_2O_5/WO_3/TiO_2$ catalysts consist of surface O=WO_4 sites on the TiO_2 support below monolayer coverage (4.5 W atoms nm^{-2}) and exhibit a W=O vibration at approximately 1010–1015 cm^{-1} that blue shifts with surface coverage from oligomerization of the surface WO_5 sites (see Figure S4). Above a monolayer surface WO_5 coverage on TiO_2 (> 4.5 W atoms nm^{-2}), crystalline WO_3 nanoparticles also form (see Figure S4). In addition, only minor shifts in the vanadyl vibration (V=O) of around 1–3 cm^{-1} are observed in Raman spectra and such peaks can be both challenging to observe and assign.

The quantitative impact of promotion by surface tungsten oxide on the SCR activity of supported 1% V_2O_5-x WO_3/TiO_2 catalysts (x = 0–8% WO_3, with 8% WO_3 corresponding to monolayer coverage) is presented in Figure 4 and shows the progressive improvement of the SCR reaction rate for the supported 1% V_2O_5-x WO_3/TiO_2 catalysts. The observed reaction rate for the supported 1% V_2O_5/TiO_2 catalyst increases by 50× with the impregnation of 8% WO_3, a value that mimics the TOF increase since the surface vanadia loading is constant. A plot of log [rate of NO_x conversion] versus log [WO_3 loading] (Figure 4) yields a slope of 1.8 reflecting the strong promotional influence of surface tungsten oxide on the SCR reaction. It is important to note that neither exposed titania sites nor surface WO_5 sites alone on TiO_2 significantly catalyze SCR of NO with NH_3 at 200 °C and higher temperatures, with titania-supported tungsten oxide demonstrating orders of magnitude lower SCR activity than titania-supported vanadia.[7,16]

Given that the surface vanadia sites are the catalytic active sites for SCR of NO with NH_3 by supported 1% V_2O_5-x WO_3/TiO_2 catalysts, the promotion mechanism of surface

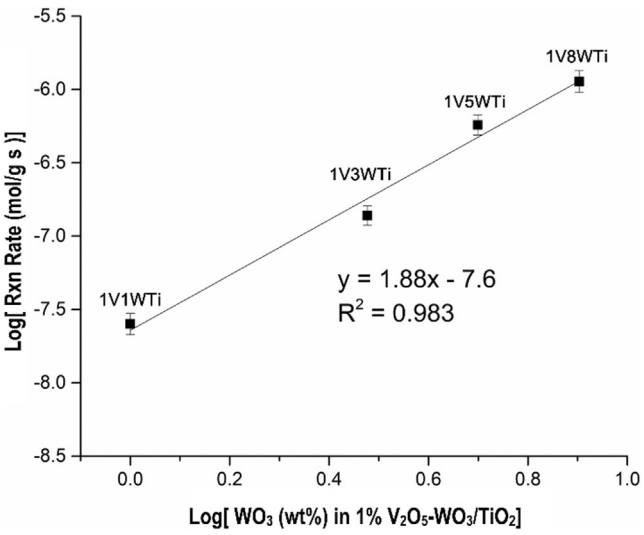

Figure 4. The log [reaction rate] versus log [tungsten oxide loading] (x axis) shows a strong correlation between tungsten oxide content and catalytic performance. Reactions were conducted at 200 °C.

tungsten oxide sites on supported V_2O_5/TiO_2 catalysts is of great fundamental and practical interest. As previously indicated, the origin of the SCR reactivity enhancements by tungsten oxide promotion has received much attention as to whether it is an electronic effect or a structural effect.[10a,25a,26] To examine the influence of the surface tungsta promoter on the structures of the surface vanadia sites, solid state ^{51}V MAS NMR was employed to compare unpromoted 1% V_2O_5/TiO_2 with promoted 1% V_2O_5-5% WO_3/TiO_2 catalysts. As shown in Figure 5 comparing promoted 1% V_2O_5-(3–5)% WO_3/TiO_2 catalysts, incorporation of surface tungsta sites to the supported 1% V_2O_5/TiO_2 catalyst results in a redistribution of the surface vanadia species in the NMR spectrum. Tungsten oxide promotion results in a spectrum revealing lines at −517 and −530 ppm (monomeric structures), a broad feature at −568 ppm from dimeric and oligomeric surface sites (which likely accounts for more than one environment due to the expansive chemical shift range), and a broad signal representing larger 2D oligomers at ≈−630 ppm. A clear enhancement of oligomeric ^{51}V NMR signals is present with the addition of tungsten oxide (ca. 53% oligomeric surface vanadia species for the W-free catalyst versus 63% and 82% oligomeric surface vanadia species for the 3% and 5% tungsta-promoted catalyst, respectively) is clearly apparent from Figure 5. Although theoretical investigations have suggested the energetic preference of VO_x/TiO_2 domains over mixed, supported VO_x-WO_x/TiO_2 mixed structures in the promoted system,[27] this does not disprove the existence of surface VO_x-WO_x dimers on TiO_2. To explore the possibility of surface VO_x-WO_x dimers on TiO_2, we evaluated a number of W^{VI}-O_x-V^V on Ti^{IV} cluster models as shown in the Supporting Information (Figure S15–16, a detailed explanation of the findings is available in the Supporting Information). Supplemental models for VO_X-WO_X dimers have some agreement on the basis of the chemical shifts, but do not fully account for all of the signals observed. Linear trimeric VOVOW structures (Figure S19), however, may reflect the observed chemical shifts as edge and central ^{51}V NMR predictions and also result in surface vanadia in close proximity to each other, satisfying the two-site requirement.

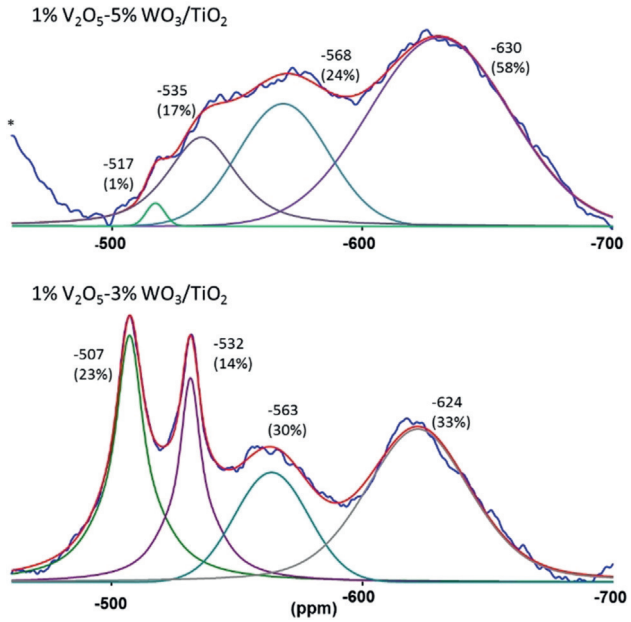

Figure 5. Solid-state ^{51}V MAS NMR spectra of dehydrated, impregnated 1% V_2O_5-(3–5)% WO_3/TiO_2 catalysts. Spectral deconvolution summation is presented by the red line, the collected data are in blue. All spectra were externally referenced to V_2O_5 at −614 ppm. Sidebands displayed are indicated by (*).

The formation of larger surface vanadia domains on TiO_2 supports in the presence of surface tungsten oxide sites have been previously proposed as a possibility on the basis of TPR, Raman, and activity measurements.[28] Raman spectroscopy, however, provided limited structural information from the slight blue shift of the V=O vibration suggesting that surface vanadia sites may become oligomerized in the presence of surface tungsta sites. The much stronger Raman band from the surface tungsta sites, however, overshadowed the weak Raman band from the surface vanadia sites making a definitive structural conclusion difficult. The current direct observation of the molecular structures of the surface vanadia sites on TiO_2 in the presence of promotion by surface tungsten oxide sites with solid state ^{51}V NMR spectroscopy clearly illustrates oligomerization of surface vanadia sites in the presence of surface tungsta sites. Further support for only a structural effect from the surface tungsta site promoter on the SCR reaction is evidenced in redox chemical probe reaction studies of SO_2 oxidation which requires only one surface vanadia active site and the fact that the reactivity of W-free and tungsten oxide-promoted supported V_2O_5/TiO_2 catalysts exhibit comparable TOF values.[29] The same reactivity for supported 1% V_2O_5/TiO_2 and 1% V_2O_5-WO_3/TiO_2 catalysts confirms the absence of electronic effects created by the presence of the surface tungsten oxide sites. The origin of the promotion by surface tungsta sites on supported V_2O_5/TiO_2 catalysts for the SCR reaction, thus, is directly observed to result from a structural effect arising from surface tungsta's role in oligomerizing the surface vanadia sites and the requirement of two adjacent surface vanadia sites for the SCR reaction as demonstrated in the present study. Further benefits of surface tungsten oxide to supported V_2O_5/TiO_2 catalysts arise from an increase in the Brønsted acidity of the catalyst, which impacts the adsorption mode of ammonia (surface NH_3 on Lewis and surface NH_4^+ on Brønsted acid sites), and a decrease in surface Lewis acid sites from the exposed titania support.[5b] The Brønsted acid sites of surface vanadia are shown to dominate the overall reaction, especially under conditions of moisture and high temperature.[5b] Although Lewis acid sites are intrinsically more active for SCR under mild conditions, they constitute only a minority of species during SCR reaction conditions.

The origin/mechanisms of the vanadia oligomerization effect by tungsten oxide remains, at present, unknown. The increased abundance of vanadia on the surface has extensively been shown to enhance the content of oligomerized species. Similarly, the addition of metal oxide (tungsten oxide) is shown to promote the formation of vanadia oligomers. It can be speculated that this observation might arise from tungsten oxide surface occupation forming local surface vanadia islands that result in high local concentrations

of oligomeric vanadia, similar to the proposed oligomerization due to a loss of available surface sites for sulfated materials.[10h,30] From this perspective, the potential surface crowding or displacement might suggest that other common, industrially relevant promoters (e.g. MoO_3) might share a similar, structural promotion effect.

Conclusion

The approach employed has outlined a strategy to assess potential structural effects of catalyst promoters and the results of this work clearly demonstrate enhanced reaction rates and TOFs with increasing surface vanadia coverage and that surface tungsten oxide addition is well correlated with the increasing amount of oligomerized surface vanadia sites. These oligomeric structures possess a greater number of adjacent surface vanadia active sites. The need for two adjacent sites for the SCR reaction is demonstrated by the relationship of rate $\approx [VO_x]^2$ for supported V_2O_5/TiO_2 catalysts with increasing surface vanadia coverage as clearly illustrated in Figure 1. The addition of surface tungsten oxide to the supported V_2O_5/TiO_2 catalysts further increases the extent of oligomerization of the surface vanadia sites and accounts for the enhanced SCR reactivity. The combination of these results has confirmed the 2-site SCR requirement and clarified the structural promoting effect of tungsten oxide on vanadia-based SCR catalysts. These new insights provide a solid understanding of the site requirements for SCR and roles of metal oxide sites and serve as a blueprint for the rational design of the next generation of catalytic SCR materials that will catalyze this important reaction for abatement of NO_x emissions from stationary sources.

Acknowledgements

The research at PNNL and The University of Alabama was supported by the U.S. Department of Energy, Office of Science, Office of Basic Energy Sciences, Division of Chemical Sciences, Biosciences, and Geosciences Catalysis Program (DE-AC05-RL01830). The research at Lehigh University was also supported by the Center for Understanding & Control of Acid Gas-Induced Evolution of Materials for Energy (UNCAGE-ME), an Energy Frontier Research Center funded by DOE, Office of Science, Office of Basic Energy Sciences under grant DE-SC0012577. Experiments were conducted in the Environmental Molecular Sciences Laboratory (EMSL), a national scientific user facility sponsored by the Department of Energy's Office of Biological and Environmental Research at Pacific Northwest National Laboratory (PNNL). NMR experiments were conducted in part using a Bruker 600 MHz NMR spectrometer acquired with support from the US Department of Energy, Office of Science, Office of Basic Energy Sciences (Project Number 66628). EMSL's supercomputers were utilized as a resource for computational modeling. Pacific Northwest National Laboratory is a multiprogram national laboratory operated by Battelle for the US Department of Energy under contract DE-AC06-76RLO 1830. The Seattle Chapter of the Achievement Rewards for College Scientists is acknowledged for their fellow sponsorship. D.A.D. also thanks the Robert Ramsay fund of The University of Alabama for support.

Conflict of interest

The authors declare no conflict of interest.

Stichwörter: Heterogene Katalyse · NMR-Spektroskopie · NO_x · Selektive katalytische Reduktion (SCR) · Vanadium

Zitierweise: *Angew. Chem. Int. Ed.* **2019**, *58*, 12609 – 12616
Angew. Chem. **2019**, *131*, 12739 – 12746

[1] K. Skalska, J. S. Miller, S. Ledakowicz, *Sci. Total Environ.* **2010**, *408*, 3976 – 3989.
[2] K. Khivantsev, N. R. Jaegers, L. Kovarik, J. C. Hanson, F. Tao, Y. Tang, X. Y. Zhang, I. Z. Koleva, H. A. Aleksandrov, G. N. Vayssilov, Y. Wang, F. Gao, J. Szanyi, *Angew. Chem. Int. Ed.* **2018**, *57*, 16672 – 16677; *Angew. Chem.* **2018**, *130*, 16914 – 16919.
[3] P. Tao, M. H. Sun, S. C. Qu, C. W. Song, C. Li, Y. Y. Yin, M. R. Cheng, *Global NEST J.* **2017**, *19*, 160 – 166.
[4] World Energy Outlook (Ed.: R. Priddle), International Energy Agency, Paris, **2016**, p. 266.
[5] a) A. Marberger, D. Ferri, M. Elsener, O. Krocher, *Angew. Chem. Int. Ed.* **2016**, *55*, 11989 – 11994; *Angew. Chem.* **2016**, *128*, 12168 – 12173; b) M. H. Zhu, J. K. Lai, U. Tumuluri, Z. L. Wu, I. E. Wachs, *J. Am. Chem. Soc.* **2017**, *139*, 15624 – 15627.
[6] J.-K. Lai, I. E. Wachs, *ACS Catal.* **2018**, *8*, 6537 – 6551.
[7] G. Busca, L. Lietti, G. Ramis, F. Berti, *Appl. Catal. B* **1998**, *18*, 1 – 36.
[8] a) M. D. Amiridis, J. P. Solar, *Ind. Eng. Chem. Res.* **1996**, *35*, 978 – 981; b) N. Y. Topsoe, J. A. Dumesic, H. Topsoe, *J. Catal.* **1995**, *151*, 241 – 252; c) N.-Y. Topsøe, *Science* **1994**, *265*, 1217; d) U. S. Ozkan, Y. P. Cai, M. W. Kumthekar, *J. Catal.* **1994**, *149*, 390 – 403.
[9] a) M. Zhu, J.-K. Lai, U. Tumuluri, M. E. Ford, Z. Wu, I. E. Wachs, *ACS Catal.* **2017**, *7*, 8358 – 8361; b) F. J. J. G. Janssen, F. M. G. Van den Kerkhof, H. Bosch, J. R. H. Ross, *J. Phys. Chem.* **1987**, *91*, 6633 – 6638; c) U. S. Ozkan, Y. Cai, M. W. Kumthekar, *J. Phys. Chem.* **1995**, *99*, 2363 – 2371; d) U. S. Ozkan, Y. P. Cai, M. W. Kumthekar, *J. Catal.* **1994**, *149*, 375 – 389.
[10] a) Y. He, M. E. Ford, M. Zhu, Q. Liu, U. Tumuluri, Z. Wu, I. E. Wachs, *Appl. Catal. B* **2016**, *193*, 141 – 150; b) W. Yu, X. Wu, Z. Si, D. Weng, *Appl. Surf. Sci.* **2013**, *283*, 209 – 214; c) A. Marberger, M. Elsener, D. Ferri, O. Kröcher, *Catalysts* **2015**, *5*, 1704 – 1720; d) B. W. Lee, H. Cho, D. W. Shin, *J. Ceram. Process. Res.* **2007**, *8*, 203 – 207; e) L. Lietti, P. Forzatti, F. Bregani, *Ind. Eng. Chem. Res.* **1996**, *35*, 3884 – 3892; f) C. Chen, Y. Cao, S. Liu, J. Chen, W. Jia, *Chin. J. Catal.* **2018**, *39*, 1347 – 1365; g) L. Lietti, I. Nova, P. Forzatti, *Top. Catal.* **2000**, *11*, 111 – 122; h) G. Z. He, Z. H. Lian, Y. B. Yu, Y. Yang, K. Liu, X. Y. Shi, Z. D. Yan, W. P. Shan, H. He, *Sci. Adv.* **2018**, *4*, eaau4637.
[11] a) X. Xiao, S. Xiong, B. Li, Y. Geng, S. Yang, *Catal. Lett.* **2016**, *146*, 2242 – 2251; b) J. P. Chen, R. T. Yang, *Appl. Catal. A* **1992**, *80*, 135 – 148.
[12] a) I. E. Wachs, *Dalton Trans.* **2013**, *42*, 11762 – 11769; b) M. A. Vuurman, I. E. Wachs, A. M. Hirt, *J. Phys. Chem.* **1991**, *95*, 9928 – 9937; c) I. E. Wachs, G. Deo, B. M. Weckhuysen, A. Andreini, M. A. Vuurman, M. deBoer, M. D. Amiridis, *J. Catal.*

1996, *161*, 211 – 221; d) G. Deo, I. E. Wachs, *J. Catal.* **1994**, *146*, 323 – 334.
[13] H. Tian, E. I. Ross, I. E. Wachs, *J. Phys. Chem. B* **2006**, *110*, 9593 – 9600.
[14] a) J. Z. Hu, S. Xu, W.-Z. Li, M. Y. Hu, X. Deng, D. A. Dixon, M. Vasiliu, R. Craciun, Y. Wang, X. Bao, C. H. F. Peden, *ACS Catal.* **2015**, *5*, 3945 – 3952; b) N. R. Jaegers, C. Wan, M. Y. Hu, M. Vasiliu, D. A. Dixon, E. Walter, I. E. Wachs, Y. Wang, J. Z. Hu, *J. Phys. Chem. C* **2017**, *121*, 6246 – 6254.
[15] a) A. Burkardt, W. Weisweiler, J. A. A. van den Tillaart, A. Schäfer-Sindlinger, E. S. Lox, *Top. Catal.* **2001**, *16 – 17*, 369 – 375; b) A. A. Shubin, O. B. Lapina, D. Courcot, *Catal. Today* **2000**, *56*, 379 – 387; c) U. G. Nielsen, N.-Y. Topsøe, M. Brorson, J. Skibsted, H. J. Jakobsen, *J. Am. Chem. Soc.* **2004**, *126*, 4926 – 4933; d) C. Gheorghe, B. Gee, *Chem. Mater.* **2000**, *12*, 682 – 685.
[16] P. R. Ettireddy, N. Ettireddy, S. Mamedov, P. Boolchand, P. G. Smirniotis, *Appl. Catal. B* **2007**, *76*, 123 – 134.
[17] M. Ek, Q. M. Ramasse, L. Arnarson, P. G. Moses, S. Helveg, *Nat. Commun.* **2017**, *8*, 305.
[18] J. M. Jehng, G. Deo, B. M. Weckhuysen, I. E. Wachs, *J. Mol. Catal. A* **1996**, *110*, 41 – 54.
[19] D. S. Kim, M. Ostromecki, I. E. Wachs, *J. Mol. Catal. A* **1996**, *106*, 93 – 102.
[20] M. O. Guerrero-Pérez, *Catalysis Today* **2017**, *285*, 226 – 233.
[21] a) H. Eckert, I. E. Wachs, *J. Phys. Chem.* **1989**, *93*, 6796 – 6805; b) V. Luca, S. Thomson, R. F. Howe, *J. Chem. Soc. Faraday Trans.* **1997**, *93*, 2195 – 2202; c) V. Y. Borovkov, E. P. Mikheeva, G. M. Zhidomirov, O. B. Lapina, *Kinet. Catal.* **2003**, *44*, 710 – 717.
[22] a) W.-Z. Li, F. Gao, Y. Li, E. D. Walter, J. Liu, C. H. F. Peden, Y. Wang, *J. Phys. Chem. C* **2015**, *119*, 15094 – 15102; b) S. Kraemer, A. J. Rondinone, Y.-T. Tsai, V. Schwartz, S. H. Overbury, J.-C. Idrobo, Z. Wu, *Catal. Today* **2016**, *263*, 84 – 90.
[23] a) Y.-J. Du, Z. H. Li, K.-N. Fan, *Surf. Sci.* **2012**, *606*, 956 – 964; b) L. Arnarson, S. B. Rasmussen, H. Falsig, J. V. Lauritsen, P. G. Moses, *J. Phys. Chem. C* **2015**, *119*, 23445 – 23452; c) L. Arnarson, H. Falsig, S. B. Rasmussen, J. V. Lauritsen, P. G. Moses, *Phys. Chem. Chem. Phys.* **2016**, *18*, 17071 – 17080.
[24] J. P. Dunn, H. G. Stenger, I. E. Wachs, *Catal. Today* **1999**, *53*, 543 – 556.
[25] a) Y. He, M. E. Ford, M. Zhu, Q. Liu, Z. Wu, I. E. Wachs, *Appl. Catal. B* **2016**, *188*, 123 – 133; b) S. Zhang, Q. Zhong, *J. Solid State Chem.* **2015**, *221*, 49 – 56.
[26] a) L. J. Alemany, L. Lietti, N. Ferlazzo, P. Forzatti, G. Busca, E. Giamello, F. Bregani, *J. Catal.* **1995**, *155*, 117 – 130; b) G. Ramis, G. Busca, C. Cristiani, L. Lietti, P. Forzatti, F. Bregani, *Langmuir* **1992**, *8*, 1744 – 1749.
[27] A. Suarez Negreira, J. Wilcox, *J. Phys. Chem. C* **2013**, *117*, 24397 – 24406.
[28] a) P. G. W. A. Kompio, A. Brückner, F. Hipler, G. Auer, E. Löffler, W. Grünert, *J. Catal.* **2012**, *286*, 237 – 247; b) C. Wang, S. Yang, H. Chang, Y. Peng, J. Li, *Chem. Eng. J.* **2013**, *225*, 520 – 527.
[29] a) J. H. Li, Y. Peng, H. Z. Chang, X. Li, J. Crittenden, J. M. Hao, *Front. Environ. Sci. Eng.* **2016**, *10*, 413 – 427; b) J. P. Dunn, H. G. Stenger, I. E. Wachs, *J. Catal.* **1999**, *181*, 233 – 243.
[30] S. T. Choo, Y. G. Lee, I. S. Nam, S. W. Ham, J. B. Lee, *Appl. Catal. A* **2000**, *200*, 177 – 188.

Manuskript erhalten: 11. April 2019
Akzeptierte Fassung online: 8. Juli 2019
Endgültige Fassung online: 1. August 2019

